Microfiber in-line Mach–Zehnder interferometer for strain sensing

C. R. Liao,[1,2] D. N. Wang,[1,*] and Ying Wang[1]

[1]Department of Electrical Engineering, The Hong Kong Polytechnic University, Hung Hom, Kowloon, Hong Kong, China

[2]College of Optoelectronic Engineering, Shenzhen University, Nanshan, Shenzhen 518060, China

*Corresponding author: eednwang@polyu.edu.hk

Received October 30, 2012; revised February 4, 2013; accepted February 4, 2013;
posted February 4, 2013 (Doc. ID 178976); published February 27, 2013

An elegant way of achieving an ultracompact optical fiber in-line Mach–Zehnder interferometer is to create an inner air cavity in a section of microfiber. The sandwich structure splits the light propagating in the fiber into two beams: one passes through the inner air cavity and the other travels along the silica wall of the cavity before recombining at the cavity end, resulting in an interference fringe pattern. Such a device is applied for strain measurement with a high sensitivity of 6.8 pm/$\mu\varepsilon$. © 2013 Optical Society of America

OCIS codes: 230.3990, 260.3160.

Strain measurement is of great importance for many applications—for example, nondestructive evaluation of civil infrastructure, structure inspection of aircraft, and earthquake monitoring. In recent years, fiber in-line interferometric sensors have been developed rapidly in strain measurement because of their compactness, high sensitivity, ease of construction, and convenient operation. Various types of fiber in-line interferometric strain–sensor configurations have been demonstrated, such as Fabry–Perot interferometers based on hollow tubes [1], femtosecond (fs) laser machined open-air cavities [2], hollow-core photonic-crystal fibers (PCFs) [3,4] or spheroidal cavities [5], and Mach–Zehnder interferometers (MZIs) based on PCFs [6], fiber taper [7], or lateral-shifted fiber splicing [8]. However, the abovementioned fiber interferometers need to use high-cost fibers, have critical requirements on interferometer specifications, or exhibit a large device dimension. Moreover, most of them have low strain sensitivity.

In this Letter, an ultracompact microfiber in-line MZI based on an inner air cavity is fabricated by combining fs laser micromachining and fusion splicing techniques. Such a device can be operated as a high-sensitivity strain–sensor with advantages of ultracompact size, low cost, and easy fabrication.

During the device fabrication process, fs laser pulses (120 fs/1 kHz/800 nm) were focused onto the fiber by an objective lens with an NA value of 0.5. A standard single-mode fiber-28 (SMF-28) (from Corning) was mounted on a computer-controlled X–Y–Z translation stage with a 40 nm resolution. The following steps were taken in the fabrication process:

(a) A microhole of a few micrometers in diameter at the center of the cleaved fiber end facet was ablated by an fs laser with on-target power of ~5 mW, as shown in Fig. 1(a). The size of the microhole determined the size and shape of the hollow sphere to be formed.

(b) The fiber tip with the microhole structure was spliced together with another cleaved SMF tip by use of a fusion splicer with a fusing current of ~16.3 mA and a fusing duration of ~2.0 s. The two splicing parameters also play an important role in determining the size and the shape of the hollow sphere and hence the air cavity in the microfiber to be formed subsequently.

(c) Since the air in the hole was suddenly heated, the hole rapidly expanded to an elliptical hollow sphere with a rather smooth surface. Its microscope side view and scanning-electron-microscope (SEM) image of a cross-section view are displayed in Figs. 1(b) and 1(c), respectively.

(d) The SMF with a hollow sphere was mounted between two translation stages and drawn into microfiber by use of a flame-brushing technique. By appropriate control of the moving speed of the flame and the holders, microfiber of different diameters could be produced, with an inner air cavity along the fiber length. The transmission spectrum was monitored during the tapering process by use of a broadband light source and an optical spectrum analyzer.

Figure 1(d) displays the microscope image of the microfiber with an inner air cavity that essentially forms a microfiber in-line MZI. In the tapered section, the input light beam is split into two portions denoted by I_1 and I_2, respectively. While I_1 travels along the silica cavity wall, I_2 propagates via the inner air cavity, and the

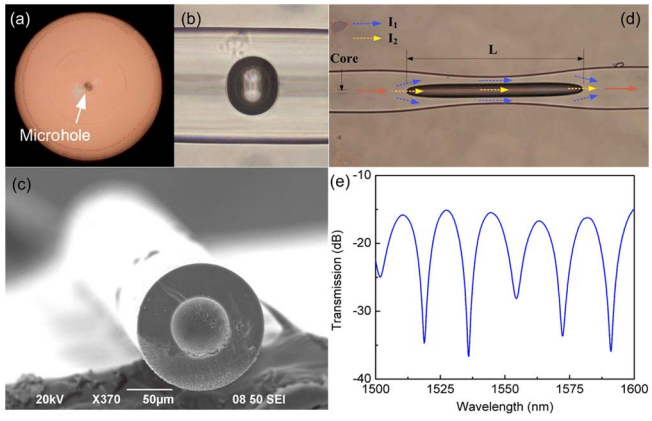

Fig. 1. (Color online) (a) Microhole fabricated by fs laser ablation at the center of the cleaved SMF end facet. (b) Hollow sphere formed after fusion splicing with another section of cleaved SMF. (c) SEM image of the cross-section view of the hollow sphere. (d) Microfiber with an inner air cavity with length L. (e) Transmission spectrum of the microfiber in (d).

0146-9592/13/050757-03$15.00/0

interference takes place when the two output beams recombine at the cavity end. The output intensity of the MZI is governed by

$$I = I_1 + I_2 + 2\sqrt{I_1 I_2}\cos\left(\frac{2\pi L\Delta n}{\lambda}\right), \quad (1)$$

where I represents the intensity of the interference signal, λ is the wavelength, L is the cavity length, $\Delta n = n_{\text{wall}} - n_{\text{hole}}$ denotes the effective refractive index (RI) difference between the two interference arms, and n_{wall} and n_{hole} are the effective RIs of the silica wall mode and the air-cavity mode, respectively. When the phase term satisfies the condition $2\pi L\Delta n/\lambda = (2m+1)\pi$, where m is an integer, the intensity dip appears at the wavelength

$$\lambda_{\text{dip}} = 2L\Delta n/(2m+1). \quad (2)$$

Thus, the free spectral range (FSR) of the spectrum can be expressed as

$$\text{FSR} = \lambda^2/(\Delta n L). \quad (3)$$

By changing the parameters used in taper drawing, microfiber MZIs with different air-cavity lengths can be created. Figure 2(b) shows three microfiber MZIs with different air-cavity lengths of 270, 570, and 860 μm, which correspond to different waist diameters of 40, 35, and 23 μm, respectively. It can be found from this figure that, with the increase of cavity length from 270 to 860 μm, the FSR around 1550 nm is decreased from 19.2 to 5.8 nm, which can be explained by Eq. (3). It can also be found that the insertion loss of the device goes up with the increase of air-cavity length. The reason is that the light propagates along the air cavity as a lossy mode and the value of loss is proportional to the propagation distance. Besides, the abrupt interface between the core and the tapered air cavity would also introduce a significant amount of loss.

To test the system response to strain variation, the three samples shown in Fig. 2 were used for comparison. All the samples were characterized in strain at room temperature, subjected to the same test condition. The fiber was attached to a translation stage with a resolution of 10 μm. The total fiber length, including SMF and microfiber, used in the experiment was 200 mm. The spectral behavior of the sample S3 around 1550 nm when axial strain is applied is displayed in Fig. 3(a), where a red spectral shift appears. The variation of the dip wavelength of different samples with axial strain between 0 to 1000 με is demonstrated in Fig. 3(b), and the results obtained clearly indicate that strain sensitivity critically depends on the shape and size of the microfiber MZI. In fact, a longer interferometer length (and hence a smaller microfiber diameter) corresponds to a higher sensitivity. The highest sensitivity obtained was 6.8 pm/με, with a length of 860 μm (S3). However, such a sample exhibits the lowest breaking strain of ~1800 με, much lower than

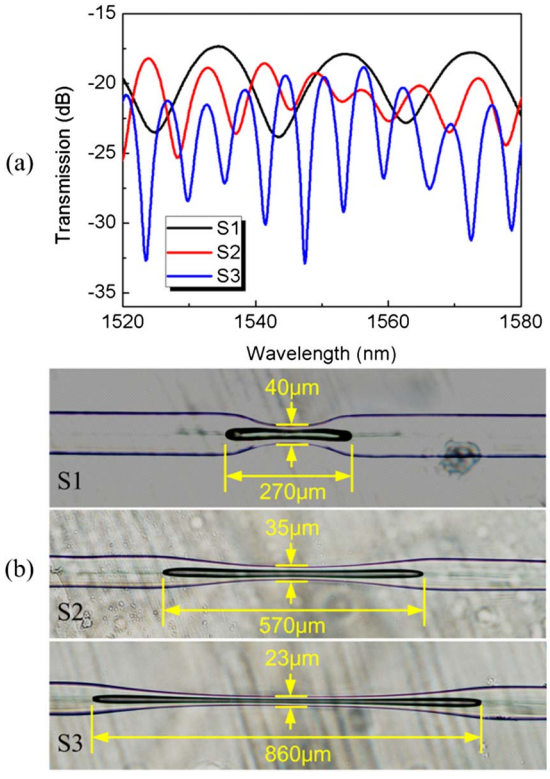

Fig. 2. (Color online) (a) Transmission spectra of microfiber MZIs with different cavity lengths of 270, 570, and 860 μm, respectively. (b) Corresponding optical microscope images of the microfiber MZIs.

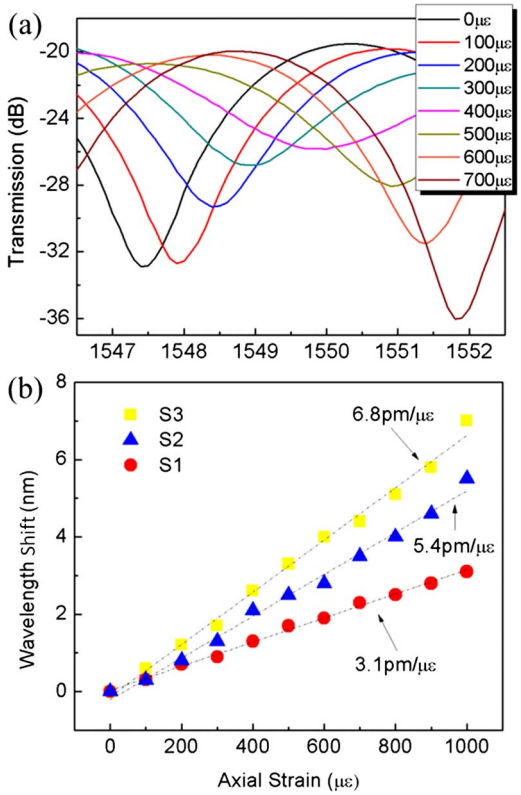

Fig. 3. (Color online) (a) Evolution of transmission spectrum of sample S3 with axial strain ranging from 0 to 700 με. (b) Variation of dip wavelength with axial strain for different samples. Linear fitting gives a strain coefficient of 3.1 ± 0.1 pm/με, 5.4 ± 0.1 pm/με, and 6.8 ± 0.2 pm/μm for samples S1, S2, and S3, respectively.

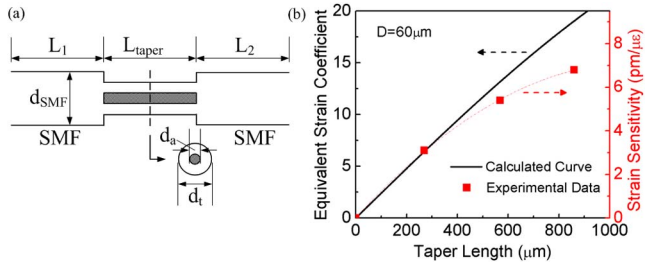

Fig. 4. (Color online) (a) Simplified model of the microfiber MZI. The shadow region is the air cavity and the cross section of the tapered region is shown in the inset. (b) Calculated equivalent strain coefficient and measured strain sensitivity variation with taper section length.

that of the SMF-based strain–sensor [9]. Thus, a good balance between strain sensitivity and robustness should be made in the microfiber-based sensor design.

The MZI proposed here is considered to be composed of a small section of hollow fiber taper connected with two sections of standard SMF. Figure 4(a) demonstrates a simplified model of the microfiber MZI where the shadow region denotes the air cavity, while the cross section of microfiber at the dashed line position is shown in the inset. Axial strain is applied to the total fiber length of $L_t = L_{\text{taper}} + L_{\text{SMF}}$, where L_{taper} stands for the taper length and L_{SMF} denotes the SMF length, i.e., $L_{\text{SMF}} = L_1 + L_2$. If strain is only applied to the taper section at a constant temperature, the interference fringe wavelength will be shifted according to

$$\Delta\lambda_{\text{MZI}} = \kappa_{\varepsilon(\text{taper})} \cdot \varepsilon_{\text{taper}} = \kappa_\varepsilon \cdot \varepsilon, \tag{4}$$

where κ_ε and $\kappa_{\varepsilon(\text{taper})}$ represent the strain coefficient of the system and the taper section, respectively; ε and $\varepsilon_{\text{taper}}$ refer to the applied strain on the system and the effective strain on the taper section, respectively [10]. When stress is applied to the entire sensor, there will be an unequal load of strain along each section of the sensor, depending on the local mechanical resistance. The strain loads applied to the hollow taper and to the SMF are equal; thus

$$\varepsilon_{\text{taper}} E A_{\text{taper}} = \varepsilon_{\text{SMF}} E A_{\text{SMF}}, \tag{5}$$

where E is Young's modulus of the fiber material, and A_{taper} and A_{SMF} are the areas of taper and the SMF cross sections, respectively. Thus, the strains applied to the two regions only depend on the ratio of the cross-section areas, according to

$$\frac{\varepsilon_{\text{taper}}}{\varepsilon_{\text{SMF}}} = \frac{A_{\text{SMF}}}{A_{\text{taper}}}. \tag{6}$$

By some algebraic manipulation, the equivalent strain coefficient can be written as

$$\frac{\kappa_\varepsilon}{\kappa_{\varepsilon(\text{taper})}} = \frac{L_{\text{taper}} + L_{\text{SMF}}}{L_{\text{taper}} + L_{\text{SMF}} \frac{V_{\text{taper}}}{L_{\text{taper}} \cdot A_{\text{SMF}}}}, \tag{7}$$

where $V_{\text{taper}} = \frac{L_{\text{taper}}\pi}{4}(d_t^2 - d_a^2)$, and d_t and d_a are diameters of the taper and air cavity respectively. In the experiment, the diameter of the hollow sphere, D, was ~60 μm, and L_{SMF} was 200 mm. Numerical simulations were performed for different taper lengths and the results obtained were compared with experimental data as shown in Fig. 4(b), where it can be found that the calculated curve and the experimental data agree reasonably well. The discrepancy generated is due to the fact that the calculated curve has good linearity when the taper section length is less than 900 μm, while the experimental strain sensitivity and the taper section length exhibit no linear relationship. The shape of the taper section is taken as uniform in the simulation but actually possesses a gradient structure.

In summary, a microfiber MZI based on inner air cavity is fabricated and used for strain sensing. The highest stain sensitivity obtained is 6.8 pm/με, corresponding to the inner air-cavity length of 860 μm. Such a microfiber device is highly sensitive, ultracompact, low cost, and simple in fabrication, which makes it attractive for many sensing applications.

This work was supported by Hong Kong government GRF (general research fund) grant PolyU 5298/10E and Hong Kong Polytechnic University research grant 4-ZZE3.

References

1. J. Sirkis, T. A. Berkoff, R. T. Jones, H. Singh, A. D. Kersey, E. J. Friebele, and M. A. Putnam, J. Lightwave Technol. **13**, 1256 (1995).
2. Y. J. Rao, M. Deng, D. W. Duan, X. C. Yang, T. Zhu, and G. H. Cheng, Opt. Express **15**, 14123 (2007).
3. Y. J. Rao, T. Zhu, X. C. Yang, and D. W. Duan, Opt. Lett. **32**, 2662 (2007).
4. M. S. Ferreira, J. Bierlich, J. Kobelke, K. Schuster, J. L. Santos, and O. Frazão, Opt. Express **20**, 21946 (2012).
5. F. C. Favero, L. Araujo, G. Bouwmans, V. Finazzi, J. Villatoro, and V. Pruneri, Opt. Express **20**, 7112 (2012).
6. B. Kim, T. H. Kim, L. Cui, and Y. Chung, Opt. Express **17**, 15502 (2009).
7. Z. Tian and S. S.-H. Yam, IEEE Photon. Technol. Lett. **21**, 161 (2009).
8. P. Lu and Q. Chen, IEEE Photon. J. **2**, 942 (2010).
9. G. Chen, H. Xiao, Y. Huang, Z. Zhou, and Y. Zhang, Proc. SPIE **7292** 729212 (2009).
10. Frazão, S. F. O. Silva, A. Guerreiro, J. L. Santos, L. A. Ferreira, and F. M. Araœjo, Appl. Opt. **46**, 8578 (2007).